Acta Metallurgica Vol. 30, pp. 297 to 310, 1982
Printed in Great Britain.

0001-6160/82/010297-14$03.00/0

DYNAMICAL SCALING OF STRUCTURE FUNCTION IN QUENCHED BINARY ALLOYS*

JOEL L. LEBOWITZ†, J. MARRO

Division de la Physique, Cen-Saclay, 91190 Gif-sur-Yvette, France; Departamento de Física Teórica y Departamento de Ecuaciones Funcionales, Universidad de Barcelona, Diagonal, 647, Barcelona-28, Spain

and

M. H. KALOS

Courant Institute of Mathematical Sciences, New York University, New York, NY 10012, U.S.A.

(*Received* 24 *February* 1981)

Abstract—We study the structure functions $S(k, t)$ obtained from computer simulations of the time evolution of a segregating binary alloy following quenching into the miscibility gap. They are shown to have a simple scaling behavior, $S(k, t) \sim K^{-3}(t)\, F(k/K(t))$. The shape of the function $F(x)$ depends somewhat on the part of the coexistence region into which the quench is made. Comparison with some recent experiments on quenched alloys is quite satisfactory. The time evolution of $K^{-3}(t)$ appears to be linear for late times, consistent with the Lifshitz–Slyozov theory.

Résumé—Nous étudions les fonctions de structure $S(k, t)$ obtenues à partir de simulations sur ordinateur de l'évolution en fonction du temps d'un alliage binaire présentant une ségrégation, après une trempe dans la lacune de miscibilité. On montre qu'elles vérifient une loi d'échelle simple $S(k, t) \sim K^{-3}(t)F(k/K(t))$. La forme de la fonction $F(x)$ dépend un peu de la partie du domaine diphasé dans lequel on fait la trempe. La comparaison avec quelques expériences récentes sur des alliages trempés est assez satisfaisante. L'évolution de $K^{-3}(t)$ en fonction du temps est linéaire après un certain temps, en accord avec la théorie de Lifshitz et Slyozov.

Zusammenfassung—Es werden die Strukturfunktionen $S(k, t)$ untersucht, die mit Rechnersimulation des Segregationsverlaufes in einer in die Mischungslücke abgeschreckten binären Legierung erhalten wurde. Diese Funktionen weisen ein einfaches maßstäbliches Verhalten auf: $S(k, t) \sim K^{-3}(t)\, F(k/K(t))$. Der Verlauf der Funktion $F(x)$ wird ein wenig von dem Koexistenzgebiet ab, in welches abgeschreckt. Ein Vergleich mit neueren Experimenten ist zufriedenstellend. Der zeitliche Verlauf von $K^{-3}(t)$ scheint für große Zeiten linear zu sein, welches mit der Theorie von Lifshitz–Slyozov übereinstimmt.

1. INTRODUCTION

The process of segregation which occurs in many alloys, e.g. Al–Zn, following quenching from the melt into the miscibility gap determines various properties of the alloy and is, therefore, of great importance. The theoretical analysis of this process, variously described as nucleation, spinodal decomposition, coarsening, and Ostwald ripening, is based mainly on the classical works of Cahn and Hilliard [1] and of Lifshitz and Slyozov [2]. The former work, as formulated by Cook [3], describes the evolution of structure function $S(k, t)$ while the latter considers the grain distribution $n(l, t)$; here t is the time since quenching, k is a reciprocal wave vector, and l is a grain size. This division corresponds directly to the two principal experimental methods of study: x-ray (or neutron) scattering for $S(k, t)$ and electron microscopy for $n(l, t)$.

Those classic works have been the subject of considerable study, criticism, extension, etc., in recent years; see e.g. the work of Langer [4], Binder [5], Furukawa [6], and others. These studies have made use of computer simulations of this process in simple model systems carried out by the authors and others [7]. A particularly striking feature of these computer experiments, observed by us recently, is the scaling behavior of the structure function, $\tilde{S}(k, t) \sim [K(t)]^{-3}\, F(k/K(t))$. A preliminary report of this work, for two quenches to low temperatures and low values of the fractional concentration of the minority component, was presented in Ref. [8]. Such scaling was also suggested independently on theoretical grounds by various authors [5, 6] and discussed in some detail by Furukawa [9].

In this note we refine and extend the scaling analysis of Ref. [8] to some new computer simulations as well as to all of our previous ones, including those at the center of the miscibility gap. We find that in *all* cases there is a scaling behavior after some initial transient time: the scaling improves with the progress of the evolution. We also find that there is a small but

* Supported in part by AFOSR Grant 78–3522 and by DOE Contract DE-AC02-76ER03077.

† Permanent address: Dept. of Mathematics and Physics, Rutgers University, Busch Campus, New Brunswick, NJ 08903, U.S.A.

apparently real and systematic dependence of the scaling function $F(x)$ on the location of the quenched state inside the miscibility gap: $F(x)$ becomes more peaked as we move away from the coexistence line. The behavior of the characteristic wave number $K(t)$ with time seems more difficult to pin down with precision. Using an asymptotic power law dependence for $K(t)$, i.e. writing $K(t) \sim t^{-a}$ for all (after the very early transients) times, the value of the exponent a appears to change from $a \simeq 0.2$ near the center of the gap to $a \simeq 0.33$ at low concentrations of one component. On the other hand for late times when scaling holds, we obtain a good fit with $K^{-3}(t) \sim A + Bt$ (See Fig. 15 and Table 3) as expected on the basis of the Lifshitz–Slyozov theory. Our guess is that the latter is indeed the right description of the phenomena for 'late times'.

The available experimental data (known to us) on real alloys is consistent with scaling behavior [10, 11]. Scaling was also found to hold in quenches of binary liquids [12]. The phenomenon therefore appears to be quite general. More precise experiments are however needed to establish conclusively this scaling behavior and clarify its features.

2. DESCRIPTION OF MODEL

The model system we study has been described before in detail [7]. At each site of a simple cubic lattice of $N = L^3$ sites ($L = 30$ or $L = 50$, in our simulations) there is assumed to be either an A atom or a B atom; the occupation variable of the ith site, $\eta(\mathbf{r}_i)$, takes on the values $+1(-1)$ when there is an A(B) atom at the lattice position $\mathbf{r}_i$. (The system is isomorphic to a lattice gas where each site can be either occupied or empty and to a ferromagnetic Ising spin system where $\eta(\mathbf{r}_i) = \pm 1$ corresponds to 'up and down' values of the spin variable). In the initial state a specified number, ρN, of randomly chosen sites are occupied by A atoms and the rest by B atoms. This corresponds to an infinite temperature state with uniform composition and no correlation between atoms at different positions. The relative concentration of A atoms is $\rho = (\bar{\eta} + 1)/2$, $0 \leqslant \rho \leqslant 1$, where $\bar{\eta} = N^{-1}\Sigma_i \eta(\mathbf{r}_i, t)$ is the average 'magnetization' in the lattice (fraction of A atoms less the fraction of B atoms), which is constant in time. The evolution proceeds by choosing, at a rate $\alpha/3$, a pair of nearest neighbor sites, i, j, in the lattice. If the sites are occupied by different kinds of atoms there is a probability

$$P_{ij} = \exp(-\beta\Delta U_{ij})[1 + \exp(-\beta\Delta U_{ij})]^{-1} \quad (1)$$

that they will be interchanged (Kawasaki dynamics [13]). Here $\beta = 1/k_B T$, k_B is Boltzmann's constant and ΔU_{ij} is the change in the energy of the system caused by the interchange.

For our model system the energy is assumed to be given by

$$U = -J \sum \eta(\mathbf{r}_i)\eta(\mathbf{r}_j), \quad J > 0. \quad (2)$$

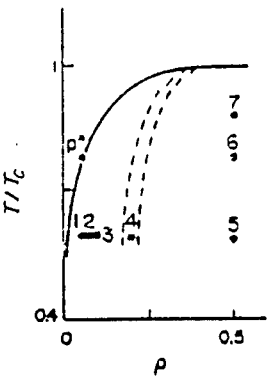

Fig. 1. Temperature-density section of the phase diagram corresponding to the infinite three dimensional binary alloy (or Ising) model. The coexistence curve (full line) is drawn according to a low-temperature series expansion and a 5/16 law near $T_c \simeq 4J/0.83686\,k_B$ (Ref. [14]). The broken lines are classical (mean-field theory) 'spinodals', supposed boundary between metastable and unstable states, according to different assumptions about the local free energy density (Reis [1] and [2]). We analyze in this paper data corresponding to the quench of our (finite) model system from an infinite temperature state to the phase points P_j, $j = 1$–7. The phase points P_1–P_5 are characterized by $T = 8J/3k_B \simeq 0.59\,T_c$ and $\rho = 0.05$, 0.075, 0.10, 0.20 and 0.50 respectively, while P_6 and P_7 (both at $\rho = 0.50$) correspond to the temperatures $T = 4J/1.137\,k_B \simeq 0.78\,T_c$ and $T = 4J/k_B \simeq 0.89\,T_c$ respectively. P^∞ is at the coexistence curve at $T \simeq 0.78\,T_c$ (and $\rho = 0.0613$).

The sum in equation (2) goes over all nearest-neighbor pairs of sites and J is positive so that the system will segregate below a critical temperature T_c. We use periodic (toroidal) boundary conditions for identifying nearest neighbors.

The phase diagram of our model A–B alloy is presented in Figure 1. For temperatures $T \geqslant T_C$ the system is uniform on a macroscopic scale at all values of ρ. For $T < T_C$ there is a range of concentrations ρ, inside the coexistence curve, for which the equilibrium state of the system is one of coexistence of two phases: one A-rich, $\rho = \rho_l$ and one A-poor $\rho = \rho_v$: $2\rho_l - 1 = 1 - 2\rho_v = m_0$, the spontaneous magnetization in spin language. The value of T_c is known very accurately for this system, $4J/k_B T_c \simeq 0.88686$, as is the whole coexistence curve [14]. The phase diagram is shown in Fig. 1. While the figure corresponds strictly to a macroscopic, formally infinite, system we expect that our system is sufficiently large for the quantities investigated to behave (for the times considered) in a manner qualitatively similar to their behavior in a macroscopic system. The absence of systematic differences between the $L = 30$ and $L = 50$ simulations appears to confirm this expectation.

2.1 *Simulations*

The dots in Fig. 1, labeled 1–7, represent, at each density, the temperature(s) inside the miscibility gap to which our model alloy was quenched from an initially random configuration (infinite temperature). They are: for P_1–P_5, $T \simeq 0.59\,T_c$ and fractional con-

Table 1.

											tend	L	NR
P_1	t	151	536	1340	2593	3899	5304	6834	8458	10,299	12,576	14,000	50	1
	k_1	0.897	0.789	0.719	0.613	0.496	0.413	0.378	0.360	0.344	0.333			
	k_2/k_1^2	1.28	1.33	1.32	1.36	1.35	1.39	1.36	1.35	1.34	1.35			
	m	35.6	52.5	72.6	106	207	321	465	539	627	699			
P_2	t	86	331	595	1159	2437	3870	5431	6633	7861	9266	10,200	50	1
	k_1	0.931	0.802	0.725	0.590	0.474	0.421	0.403	0.382	0.372	0.365			
	k_2/k_1^2	1.23	1.26	1.29	1.33	1.32	1.29	1.28	1.29	1.30	1.30			
	m	37.4	67.9	92.1	164	330	449	531	598	622	648			
P_3	t	55	227	630	1313	2062	3010	3720	4807	5836	6970	7300	50	1
	k_1	0.973	0.846	0.706	0.587	0.543	0.501	0.481	0.447	0.438	0.415			
	k_2/k_1^2	1.19	1.22	1.23	1.24	1.24	1.24	1.24	1.26	1.25	1.26			
	m	39.1	72.6	130	212	271	330	386	438	490	536			
P_4	t	28	110	250	574	934	1320	1721	2132	2705	3593	3900	30	8
	k_1	1.048	0.908	0.799	0.694	0.634	0.601	0.576	0.552	0.528	0.491			
	k_2/k_1^2	1.15	1.16	1.17	1.17	1.17	1.17	1.17	1.17	1.18	1.18			
	m	26.1	44.2	67.6	107	133	155	172	187	210	234			
P_5	t	12	28	41	64	130	216	309	406	508	560	650	30	8
	k_1	1.107	1.065	1.038	0.983	0.895	0.831	0.783	0.747	0.717	0.705			
	k_2/k_1^2	1.14	1.14	1.13	1.13	1.13	1.13	1.13	1.13	1.13	1.13			
	m	21.3	30.6	35.7	43.6	59.0	73.0	84.6	96.1	107	112			
P_6	t	16	56	190	409	795	955	1117	1281	1446	1614	1700	36	8
	k_1	1.091	0.950	0.787	0.685	0.603	0.578	0.555	0.538	0.520	0.504			
	k_2/k_1^2	1.13	1.14	1.16	1.17	1.18	1.18	1.19	1.19	1.19	1.19			
	m	23.2	40.3	68.6	102	136	149	161	176	195	208			
P_7	t	117	301	586	1144	1773	2589	3415	4245	5085	6357	6600	36	8
	k_1	0.849	0.690	0.584	0.502	0.448	0.418	0.393	0.369	0.349	0.327			
	k_2/k_1^2	1.13	1.18	1.23	1.25	1.26	1.27	1.27	1.29	1.29	1.31			
	m	47.8	76.1	104	149	192	221	250	290	310	343			
Au–60% Pt	t(sec)	0(?)	30	60	120	360	600	900						
$T \simeq 0.6\ T_c$	$k_1 \times 10^6$	11.5	11.93	11.56	11.26	10.49	10.15	9.74	—	—	—			
Ref. [10]	k_2/k_1^2	1.20	1.12	1.12	1.12	1.12	1.12	1.12						
	$p' \times 10^{10}$	18,285	90,887	94,788	99,169	107,567	113,390	119,100						

Values of k_1, k_2/k_1^2 (see equation (14)) and

$$m(t) \equiv \sum_{k=2\pi/L}^{k=0.55a} S_1(k,t)$$

at selected values of the time (in units of α^{-1}) for the quenches to P_1–P_7. Note that k_1 and k_2 refer to the quantity $S_1(k,t)$, using the values of $m(t)$, the definition equations (13) and the values in Table 2, one can however obtain k_1 and k_2 referring to $S(k,t)$. t_{end} is the latest time (in units of α^{-1}) monitored during the corresponding evolution, L refers to the size of the model system, and NR is the number of independent runs made at that particular phase point. We have also included for comparison values for k_1, k_2/k_1^2 and $p(t) \equiv \sum S(k,t)$, where the sum is restricted to the visible zone of $S(k,t)$, computed from the data in Fig. 3 of Ref. [10] corresponding to the Au–60 at.% Pt alloy quenched to $T \simeq 0.6\ T_c$. In this case $0.03\ \text{Å}^{-1} \leq k \leq 0.21\ \text{Å}^{-1}$, and the values are given in c.g.s. units.

centration of A-atoms $\rho = 0.05, 0.075, 0.10, 0.20$ and 0.50 respectively. At this temperature the value of ρ at the coexistence line is $\rho_0 \simeq 0.015$, $m_0 \simeq 0.97$. The points P_3 and P_4 are at $\rho = 0.5$ and $T = 0.78\ T_c$ and $T = 0.82\ T_c$ [illegible] T_c, $\rho_0 \simeq 0.013$, $m_0 \simeq 0.977$, while at those [illegible] $\rho_0 \simeq 0.03$, $m_0 \simeq 0.93$.

The evolution of the system following quenching was observed up to a time t which varied between about $10^3\,\alpha^{-1}$ and $10^4\,\alpha^{-1}$ (see Table 1). α^{-1} is the average time interval between two attempts at exchanging a specific site and is taken as our time unit. To make some comparison with experiment we need at least a rough idea of how to compare time scales. We do this by noting that in our model the diffusion coefficient of a single A atom in a crystal of B atoms is given by $D = \alpha/6$ since the probability that a given bond will be tried in time dt is $(1/3)\,\alpha\,dt$ and if tried the probability of an exchange is 1/2. We therefore think of our time unit at temperature T as comparable to $a_0^2/6D_0(T)$ where a_0 is the lattice spacing and $D_0(T)$ is the diffusion constant of a real alloy at temperature T in the limit of zero concentration of A atoms. The lattice spacing a_0 is our unit of length. The relevant parameters for the Al–Zn alloys are estimated [21] to be $a_0 \simeq 3$ Å, $T_c \simeq 350$°C and $D_0 \sim 10^{-18}$ cm^2/s at $T = 0.59\ T_c$. According to this rough estimate, the physical time interval in our studies at P_1 to P_5 is many hours. This is however only an order of magnitude computation since defects, vacancies and other imperfections built in during quenching may greatly speed up the time in a real alloy.

2.2 *Structure function*

The quantity of primary interest in our observations was $S(\mathbf{k}, t)$, the structure function at time t following quenching. $S(\mathbf{k}, t)$ is the Fourier transform of the spatial correlation function $G(\mathbf{r}, t)$:

$$S(\mathbf{k}, t) = N^{-1}\left\langle \left| \sum_j \exp(i\mathbf{k}\cdot\mathbf{r}_j)[\eta(\mathbf{r}_j, t) - \bar{\eta}] \right|^2 \right\rangle = \sum_{\mathbf{r}} \exp(i\mathbf{k}\cdot\mathbf{r})\,G(\mathbf{r}, t), \tag{3}$$

$$G(\mathbf{r}, t) = N^{-1} \sum_i \langle [\eta(\mathbf{r}_i, t) - \bar{\eta}][\eta(\mathbf{r}_i + \mathbf{r}, t) - \bar{\eta}] \rangle, \tag{4}$$

where $\mathbf{r}$ and $\mathbf{r}_i$ run over the N lattice sites and $\mathbf{k} = (2\pi/L)\mu$, $\mu_\alpha = 0, \pm 1, \ldots, \pm L/2$, $(\alpha = 1, 2, 3)$, specifies the first Brillouin zone. The $\langle\ \rangle$ represents an ensemble average which could in principle be implemented on the computer by making many independent runs. In practice we used between one and eight independent runs and relied on the spatial averaging given in equation (4) as well as on some 'time averaging' for obtaining reliable data; see end of section.

$S(\mathbf{k}, t)$ is periodic in each component with period $2\pi/L$; $S(\mathbf{k} = 0, t) = 0$ and

$$N^{-1} \sum_{\mathbf{k}} S(\mathbf{k}, t) = (1 - \bar{\eta}^2). \tag{5}$$

The above statements hold exactly for any 'run'. We expect also, that apart from small fluctuations, each run started at $t = 0$ with a random configuration will have

$$S(\mathbf{k}, 0) \simeq (1 - \bar{\eta}^2),\ \mathbf{k} \neq 0 \tag{6}$$

and that $S(\mathbf{k}, t)$ will have cubical symmetry for $t > 0$.

In order to reduce our data to a manageable level as well as to compare with experiments on polycrystalline materials we define an average structure function depending only on the wave number $k \equiv 2\pi\mu/L$, $\mu = 0, 1, \ldots, \sqrt{3}\,L/2$,

$$S(k, t) = \sum_{[k]} S(\mathbf{k}, t) \Big/ \sum_{[k]} 1 \tag{7}$$

where

$$\sum_{[k]}$$

is the sum over all values of $\mathbf{k}$ in the first octant, $k_\alpha \geqslant 0$, $\alpha = 1, 2, 3$, such that

$$(2\pi/L)(\mu - 1/2) \leqslant |\mathbf{k}| \leqslant (2\pi/L)(\mu + 1/2). \tag{8}$$

Note that the average defined in equation (7) is not exactly a spherical average since the points on the boundary and in the interior of the first octant of the Brillouin zone are given equal weights. Thus if $n(k)$ is the actual number of points in the first Brillouin zone contained in the full spherical shell specified in (8), then $n(k)$ is less than $8\ n_+(k)$;

$$n_+(k) \equiv \sum_{[k]} 1$$

is 1, 6, 13, 19, 39, 55, 72, 91, 114, 169, 178, 210, 253, 306, 346, ... in successive shells. Using the sum rule equation (5) we should have

$$(1 - \bar{\eta}^2)N^{-1} \sum_{k=0}^{\sqrt{3}\pi} n(k)S(k, t) = 1. \tag{9}$$

Any deviations from this sum rule in our actual runs, using $n_+(k)$, should be due primarily to fluctuations in $S(k, t)$ for any run among the different octants of the Brillouin zone and only secondarily to our choice of spherical averaging. Both of these effects become negligible for large N and we expect them to make only a small difference in our simulations, since all our results involve some averaging.

Typically, the 'sphericallized' structure function $S(k, t)$ and the other quantities of interest (such as cluster properties, etc; see later on) were computed during the simulation after every 50,000 actual exchanges (more frequently during the initial regime). Then, to obtain a smoother behavior with time, and extract the essential features, 20 different consecutive values in time were averaged leaving us with a few values (between 10 and 25) at different times from which our graphs and tables were computed. The data corresponding to our simulations at P_4–P_7,

where the $N = 27{,}000$ lattice was used, comes (in addition) from an average over eight independent runs, i.e. eight evolutions starting with independent, initial random configurations. The data at P_1–P_3 (and at the other phase points mentioned in the text but not included in Fig. 1) comes from one evolution on the $N = 125{,}000$ lattice.

3. DISCUSSION OF RESULTS

3.1 *Qualitative behavior of* S(k, t)

In our simulations we were able to monitor $S(k, t)$ for 10 shells, $\mu = 1, \ldots, 10$, for the $L = 30$ lattice used at points P_4 to P_7 and for 14 shells in the $L = 50$ lattice used for P_1 to P_3.

Figure 2 shows plots of $S(k, t)/(1 - \bar{\eta}^2)$ vs k at different times for quenches to the point P_1. These plots are qualitatively similar to those obtained at other points P_n. At $t = 0$, the system is completely disordered and $S(k, 0)/(1-\bar{\eta}^2) \sim 1$ independent of k; see equation (6). The system is then quenched to some low temperature inside the coexistence curve. Thermal processes lead to the migration of A and B atoms, proceeding (in our model) via nearest neighbor exchanges given by the transition probability equation (1), which now drive the system towards equilibrium corresponding to segregation into A-rich and B-rich regions. As these regions grow in size, $S(k, t)$ develops a peak at $k = k_{max}(t) \cong \pi/R(t)$ where $R(t)$ represents some characteristic length in the system at time t following the quench. This length will grow in time as the single phase regions grow to macroscopic sizes so that $k_{max}(t) \to 0$ as $t \to \infty$ in a macroscopic system. (In the computer simulations we obviously have $R(t) < \frac{1}{2}L$.) For contrast we also show, in Fig. 3, the qualitatively very different behavior of $S(k, t)$ when the system is quenched to the point P^*, $\rho = 0.0613$, $T \cong 0.78\ T_c$, at the coexistence curve.

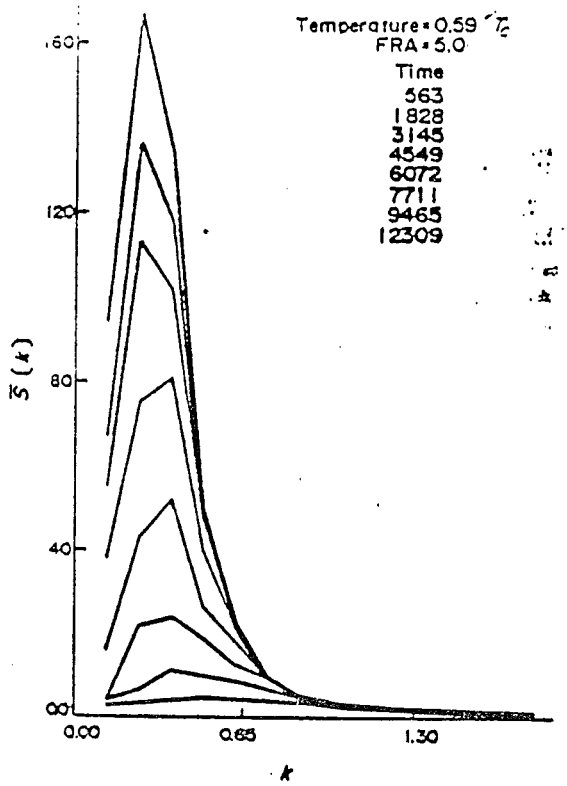

Fig. 2. Development with time of $\bar{S}(k, t) \equiv S(k, t)/(1-\bar{\eta}^2)$ vs k (in units of a_0^{-1}, a_0 being the lattice spacing) at different times in the case of a quench of the model system with $N = 125{,}000$ sites to the phase point P_1. Note that, in this case, we only have $\bar{S}(k, t)$ at fourteen different values of k, $k = 2\pi\mu/50$, $\mu = 1$–14, which have been connected by straight lines. Increasing values of the time, in units of α^{-1}, the average time internal between two attempts at exchanging a specific site, correspond to the different graphs from the bottom of the picture to the top. The graphs at different values of the time tend to form a common envelope for $k > k_{max}$, the location of the maximum intensity (which is shifting with time towards smaller values of k). This is in contrast with the cross-overs characterizing the tail $k > k_{max}$ of the $\bar{S}(k, t)$ vs k curves in the case of quenches to P_4 (Fig. 2, Ref. 7c) and to P_5 (Fig. 2, Ref. [7a]).

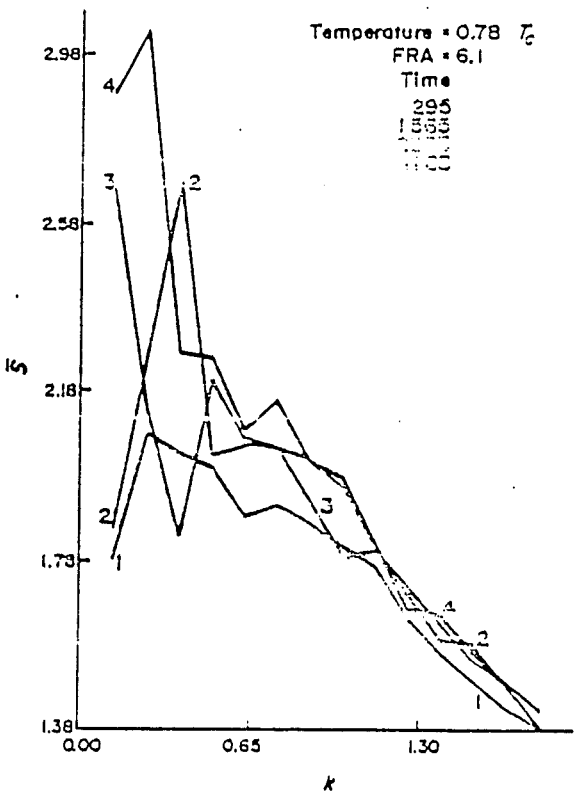

Fig. 3. Same as Fig. 2 in the case of a quench to P^*, $T \cong 0.78\ T_c$, $\rho = \rho_c(T) = 0.0613$, i.e. on the coexistence line at the same temperature as P_4. A comparison with Fig. 2 shows up how the model system differentiates P^* from P_1, say. (Note that the ordinate scale differs by two orders of magnitude). Here increasing values of the time, in units of α^{-1}, correspond to increasing values of the number labeling the different graphs.

One striking difference between the different quenches is the time, in units of α^{-1}, it takes the system to achieve a certain amount of segregation, as reflected in the development of $S(k, t)$. A crude but simple quantitative measure of this is obtained by considering the quantity

$$p(t) \equiv [(1 - \bar{\eta}^2)N]^{-1} \sum_{k=0}^{\mathcal{N}} n(k) S(k, t) \qquad (10)$$

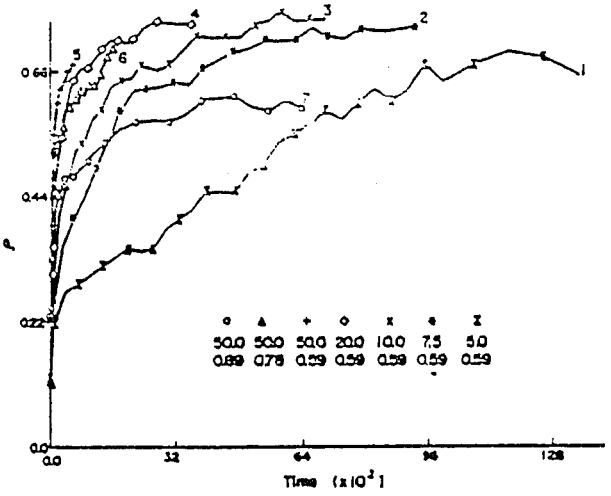

Fig. 4. The quantity $p(t)$ defined in equation (10) is plotted here vs time (note that the horizontal axis is labeled in units of $100\,\alpha^{-1}$) in the case of the quenches to P_j, $j = 1$–7. The corresponding value of j identifies each line which is also identified by different symbols. Below each symbol the values of the corresponding percentage of A-atoms and of the ratio T/T_c, respectively, are also shown. Note that the sums defined in equations (10), (14) and (19) actually go from $k = 2\pi/L$ to $k = \mathcal{K} \simeq 0.55\pi$; we have precisely $\mathcal{K} = 8\pi/15$ for $L = 30$ (so that the sum includes 8 different values) and $\mathcal{K} = 14\pi/25$ for $L = 50$ (14 different values).

where $\mathcal{K}$ is some cut-off, less or equal to the largest value of k studied in our simulations which was $2\pi/3$ for $L = 30$ and $14\pi/25$ for $L = 50$. At $t = 0$, $p(0)$ is just equal to the fraction of points of the first Brillouin zone which are contained in $|\mathbf{k}| \leq \mathcal{K}$. Choosing $\mathcal{K} \cong 0.55\pi$ in both cases (dropping the last two shells for $L = 30$) this corresponds to $p(0) \cong 0.1$. As t increases and the weight of S shifts toward smaller values of k, $p(t)$ increases by the 'amount' of $S(k, t)$ which has moved into the 'observation' zone defined by the cut-off $\mathcal{K}$. Fig. 4 shows $p(t)$ vs t for different quenches. Comparisons of the graphs for points P_1 to P_5 shows that the speed of the segregation increases, in units of attempted exchanges, with the distance of the quench from the coexistence line. The same is true for the points P_5 to P_7. This accounts, in the main, for the widely different time lengths to which we ran our simulations (see Table 1). It is clear that close enough to the coexistence line at $T \simeq 0.6\,T_c$ the relaxation time would become so long that the system would appear, for all practical purposes, to be in a metastable state while close to T_c the system will be in the region of critical slowing down. In either case the segregation would not be visible in our simulations.

It should be noted that the relaxation time increases rapidly as one approaches the coexistence line.

There is no evidence, however, in our simulations of any *abrupt* change in the behavior on crossing any of the theoretical spinodal lines indicated in Fig. 1. There are some differences however in the way in which $S(k, t)$ evolves with time in different parts of the coexistence region. This can be seen in Figs 5 and 6

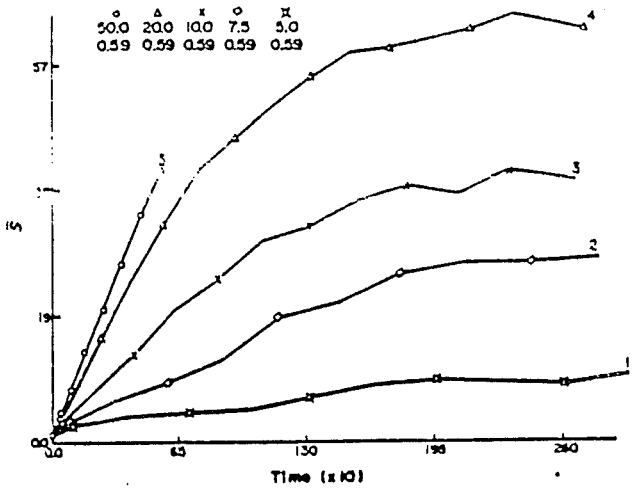

Fig. 5. The normalized structure functions $S(k, t) \equiv S(k, t)/(1-\bar{\eta}^2)$ is plotted here vs time in the case of the quenches to P_j, $j = 1$–5 ($T \simeq 0.6\,T_c$), for $k = \pi/5$.

where we plot $S(k, t)/(1 - \bar{\eta}^2)$ vs t for quenches to different P_j's at $T \simeq 0.6\,T_c$ for $k = \pi/5$ and $k = 2\pi/5$. It is seen there that for quenches deep in the coexistence region $S(k, t)$ decreases strongly after reaching its maximum value while near the coexistence line it remains approximately constant for the times observed. This behavior is also true for other values of $k > k_{max}$ and results in 'cross-overs' at large k seen in $S(k, t)$ vs k curves, for P_4 in Fig. 2(a) of Ref. [7c] and for P_5 in Fig. 2 of Ref. [7a] but not in Fig. 2 here. Such cross-overs have been conjectured [4] to be the hallmark of quenches inside the spinodal curve and our simulations give some evidence of this. The evidence is however not entirely conclusive since the differences may be due to not waiting 'long enough' near the coexistence line and the scatter is relatively large (see e.g. Figs 3–4 in Ref. [7a] corresponding to the quenches to P_6–P_7).

3.2 *Scaling behavior of* S(k, t)

An inspection of Fig. 2 shows clearly that the wide

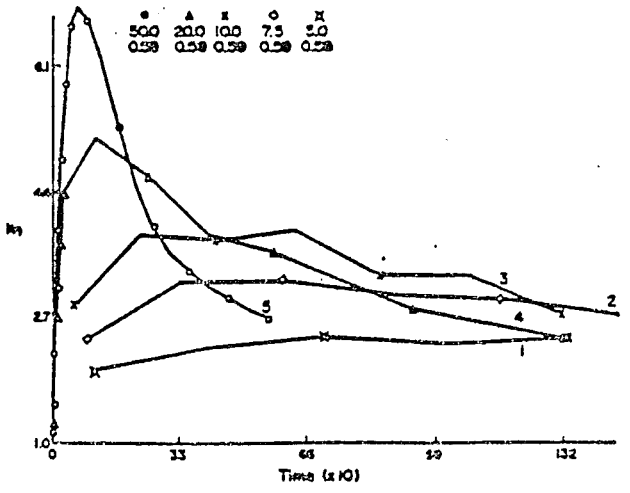

Fig. 6. Same as Fig. 5 for $k = 2\pi/5$.

spacings of possible k values coupled with fluctuations, both due to the small size of our model system, make detailed comparisons between the $S(k, t)$ obtained from our simulations and the smooth structure functions seen in experiments [10–12] or obtained from theory [3–6] very difficult. The latter always deal with macroscopic size systems which corresponds in our model to $N \to \infty$, k becoming a continuous variable and $S(k\,t)$ a continuous function of k. Let $\mathcal{S}(k, t)$ be the limit of $S(k, t)$ as $N \to \infty$. It is this smooth function about which we would like to obtain information from our computer simulations. Hence it is essential that we look for quantitative features in our computed $S(k, t)$ which will go over smoothly to the macroscopic $\mathcal{S}(k, t)$.

In order to understand the long time behavior of $\mathcal{S}(k, t)$ we note that as $t \to \infty$ we expect that $\mathcal{S}(k, t) \to$ [illegible] equilibrium structure function of a macroscopic system that segregated into two pure phases. This is given by

$$\mathcal{S}_{eq}(k) = (m_0^2 - \bar{\eta}^2)\bar{\delta}(k) + \mathcal{S}_e(k; T) \qquad (11)$$

where $\bar{\delta}(k)$ is the sphericalized Dirac delta function at $k = 0$, $\mathcal{S}_e(k; T)$ is the equilibrium structure function on the coexistence line (by the symmetry of our model system this is the same for both pure phases) and $m_0(T)$ is the spontaneous magnetization, $m_0 = 1 - 2\rho_v = 2\rho_l - 1$ (equal to $\bar{\eta}$ on the coexistence line). As already noted, the system, after quenching, will segregate locally into regions (often referred to as grains, clusters or droplets) of A-rich and B-rich phases and then will evolve further by the growth of these segregated regions (coarsening or Ostwald ripening). We might expect that after some initial time the structure function 'within' the segregated regions will be close to its equilibrium value $\mathcal{S}_e(k; T)$. It seems therefore reasonable to consider the quantity

$$\mathcal{S}_1(k, t) = [\mathcal{S}(k, t) - \mathcal{S}_e(k; T)]\,(m_0^2 - \bar{\eta}^2)^{-1}, \quad (12)$$

which approaches $\bar{\delta}(k)$ with time, as most relevant for the description of the coarsening process. This is basically the subtraction of 'background' proposed in the third reference of Ref. [5].

We shall therefore consider in our analysis also the analogous quantity for our finite system

$$S_1(k, t) \equiv [S(k, t) - S_e(k; T)]\,(m_0^2 - \bar{\eta}^2)^{-1} \quad (13)$$

in the hope that it will more clearly reveal the essential features of the coarsening process. The function $S_e(k; T)$ was obtained, for the three different temperatures T considered here, by quenching to points on the coexistence line and waiting for the system to reach equilibrium. At low temperatures there is in fact very little difference between S and S_1 for small values of k after some initial times. (c.f. Figs. 2 and 3; see also Table 2). The difference is therefore likely to be unimportant also experimentally; but it appears to help with the proper normalization of our data at different points P_ρ. It also makes some difference for P_7 where $T = 0.89\,T_c$ and $S_e(k; T)$ is not so negligible at the relevant k values; see table 2.

Table 2.

T/T_c	ρ_v	p	k_1	k_2	m
0.591	0.01456	0.13	0.922	1.105	17.8
0.780	0.06130	0.17	0.849	0.966	27.7
0.887	0.012463	0.22	0.744	0.786	43.5

Equilibrium values of the first and second moments of $S_e(k)$, and the quantity

$$m \equiv \sum_{k=2\pi/L}^{1.4\pi/2\delta} S_e(k)$$

and p defined in equation (10) corresponding to quenches to the coexistence curve at the temperatures of the simulations reported in this paper.

A quantitative feature of $S(k, t)$ we looked at in our simulations were the moments

$$k_n(t) = \langle k^n \rangle = \sum_{k=0}^{\varkappa} k^n S_1(k, t) \Big/ \sum_{k=0}^{\varkappa} S_1(k, t), \quad n = 1, 2 \qquad (14)$$

where $\varkappa \simeq 0.55\pi$ as explained before (see caption for Fig. 4). These appeared to behave quite smoothly as functions of t. We found furthermore that $\langle k^2 \rangle / \langle k \rangle^2$ was essentially independent of t; see Table 1. This suggests that our $S_1(k, t)$ with discrete argument k having spacings $2\pi/L$ might be related for late times to the macroscopic structure function $\mathcal{S}_1(k, t)$ via a smooth scaled function $\mathcal{F}$ such that

$$S_1(k, t) \cong \mathcal{S}_1(k, t) = b(t)\mathcal{F}(k/K(t)) \qquad (15)$$

where $K(t)$ is some characteristic wave vector in the system and $b(t)$ is a normalizing factor. Now if this is indeed the case, then using the fact that for large systems the number of points in the Brillouin zone contained in a spherical shell of thickness Δk approaches $4\pi k^2 \Delta k/(2\pi/L)^3$, we have from equations (9) and (12) that

$$\int_B k^2 \mathcal{S}_1(k, t)\,dk = b(t)K^3(t) \int x^2 \mathcal{F}(x)\,dx = 2\pi^2(m_0^2 - \bar{\eta}^2) \qquad (16)$$

independent of t. The integration on the left side of equation (16) is over the first Brillouin zone and so the x integration is over a cube centered at the origin with sides of length $2\pi/K(t)$. For large t, $K(t) \to 0$, and the integral in (16) can be taken over all space. Since $\mathcal{F}(x)$ can be expected to decay quite fast for large x very little error will be made even at quite early times if we set $b(t) = 2\pi^2 K^{-3}(m_0^2 - \bar{\eta}^2)$ and normalize $\mathcal{F}$ so that

$$\int_0^\infty x^2 \mathcal{F}(x)\,dx = 1. \qquad (17)$$

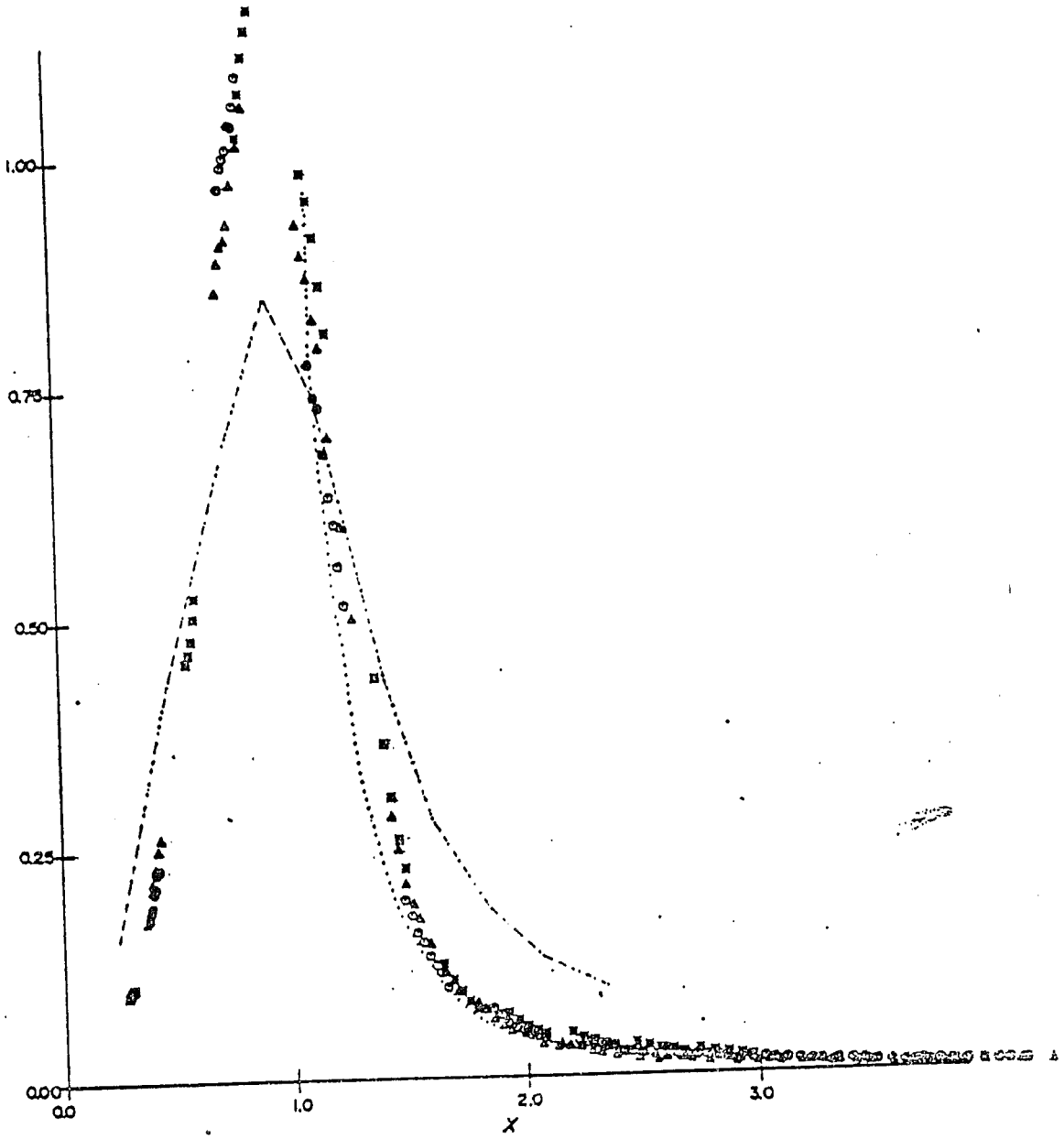

Fig. 7. The scaling function $F(x)$ in the case of 'deep' quenches: the triangles correspond to a quench to P_4 and they include times $t \geqslant 1500\,\alpha^{-1}$, the asterisks to P_3 and $t \geqslant 350\,\alpha^{-1}$, and the circles to P_6 and $t \geqslant 1000\,\alpha^{-1}$ (see also caption for Fig. 8). The dashed line represents the shape of the function F at an earlier time when scaling does not yet hold: it was drawn connecting the discrete values of $F(x;t)$ for $t = 110\,\alpha^{-1}$ in the case P_4. The dotted line corresponds to a function $F^{-1} = \alpha_1 + \alpha_2 x^4$ trying to fit the experimental data for $x > x_{max}$, the location of the maximum of $F(x)$.

To test this scaling hypothesis and find the smooth $\mathcal{F}(x)$ from our simulations we *define* a function of two variables, $x = k/k_1(t)$ and t, by the relation

$$F(x;t) \equiv \frac{L}{\pi} k_1^3(t) S_1[x k_1(t), t] \Big/ \sum_{k=0}^{\pi} k^2 S_1(k,t) \qquad (18)$$

and then see whether for late times $F(x;t) \simeq F(x)$ a smooth function of x independent of t. The normalization (18) is chosen so that

$$\sum_{j=1}^{\pi/\delta} (j\delta)^2 F(j\delta;t)\delta = 1 \qquad (19)$$

independent of t for $\delta = 2\pi/k_1(t)L$. This means that if scaling is really valid then for large N, when equation (19) approximates the corresponding integral, it will satisfy equation (17). (Note that equation (18) is defined slightly differently, using S_1 rather than S and multiplying by L/π, than the corresponding function for P_2 and P_3 in Ref. [8]).

The values of $F(x;t) \cong F(x)$ independent of t, obtained from our simulations for large times are shown in Figs 7–9 for 'deep', 'intermediate' and 'shallow' quenches. While these curves are all similar, the 'experimental' scatter within each group is signifi-

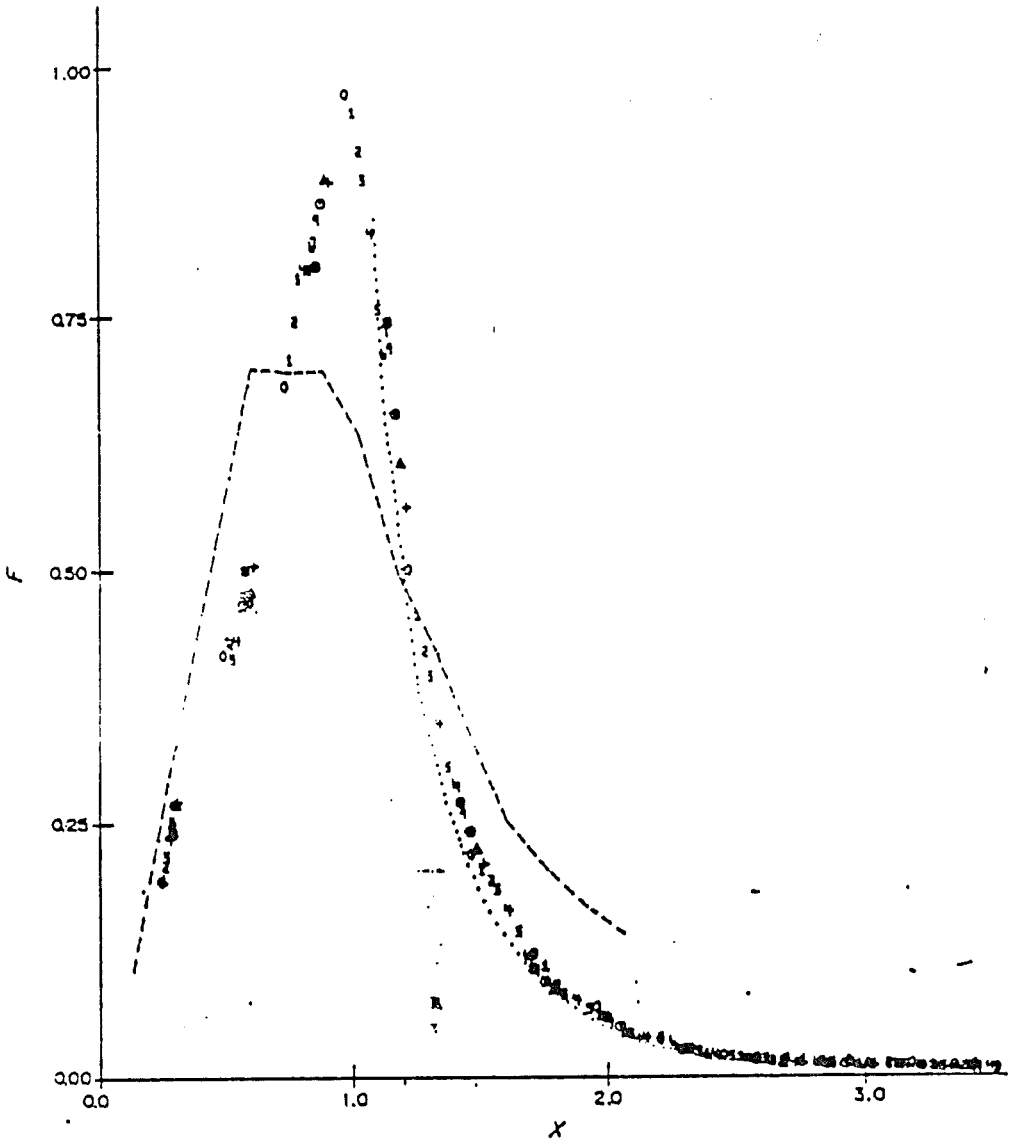

Fig. 8. The function $F(x;t)$ defined in equation (18) is plotted here versus $x = k/k_1(t)$ in the case of the ('intermediate') quench to P_3. Every symbol (0, 1, 2, 3, ...) in the graph corresponds to a different value of the time: the first one (zero) is for $t \simeq 2500\,\alpha^{-1}$, the time increasing up to $t \simeq 7300\,\alpha^{-1}$ which is represented by crosses. All the values of $F(x;t)$ in that time interval seem to lie on a common curve at different values of x (see, however, Fig. 12). The dashed line was drawn connecting the values of $F(x,t)$ at $t = 228\,\alpha^{-1}$. The dotted line corresponds to a fit $F^{-1} = \alpha_1 + \alpha_2\, x^4$ to the 'tail' $x > x_{max}$ of $F(x)$.

cantly smaller than between them. We believe therefore that there is a real, albeit small, difference between the scaling function $F(x)$ at different quenches.

The change in the scaling function may perhaps be explained by the difference in the boundaries of the single phase regions changing from smooth to corrugated as we get closer to the critical point. The similarity of $F(x)$ near T_c and near the coexistence curve for small ρ would appear to suggest some sort of 'spinodal line' criticality. This is an intriguing question which is however very difficult to answer at present.

Figures 7–9 also show the function $F(x;t)$ at some earlier times as indicated. We have also included in those figures a fit of the form $(\alpha_1 + \alpha_2 x^4)^{-1}$ to the 'tail', $x > x_{max}$ of the scaling function $F(x)$ which seems to be suggested by Ref. [9]. While this is approximately the behavior of our data for $x \gtrsim x_{max}$, the location of the maximum of $F(x)$, the data clearly deviates from the x^{-4} behavior at larger x values. This is shown in Fig. 10 where we have plotted F^{-1}, $x > x_{max}$, versus x^4 in the case of the quench to P_4. The graphs in Fig. 10 also show that $F(x;t)$ has not yet reached the assymptotic function $F(x)$ at large values of x in our simulations so this may be a part of the reason for the observed deviations from the x^{-4} behavior.

As already mentioned it is a difficult task to extract from our simulations precise and reliable information

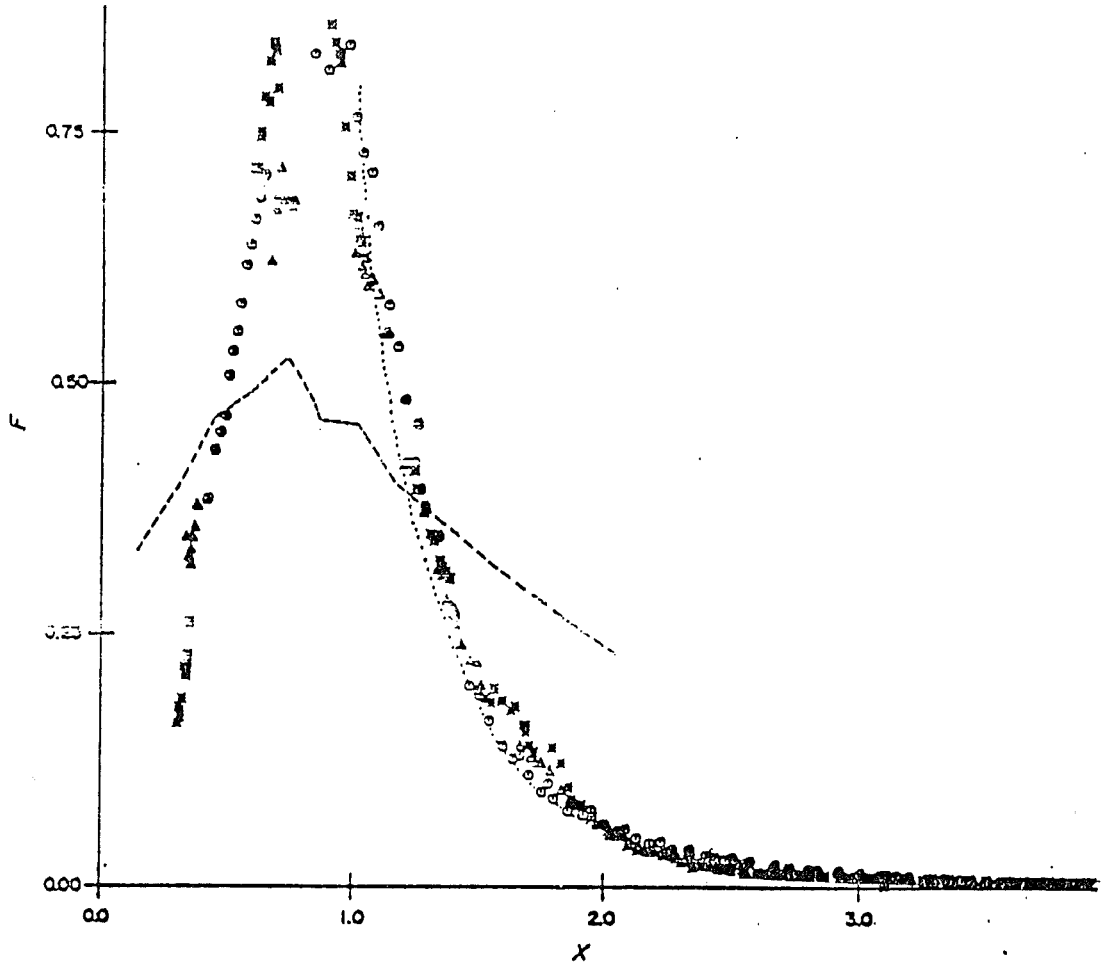

Fig. 9. Same as Fig. 7 in the case of ('shallow') quenches to P_1 (triangles; all the data $t \geqslant 6800\,\alpha^{-1}$ is included in this case), P_2 (asterisks, $t \geqslant 4000\,\alpha^{-1}$) and P_7 (circles, $t \geqslant 1000\,\alpha^{-1}$). The dashed line is for P_1 and $t = 209\,\alpha^{-1}$.

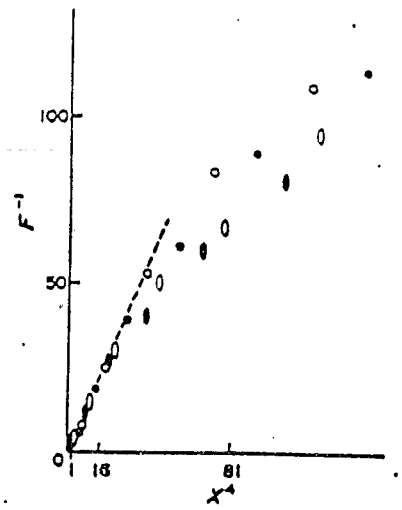

Fig. 10. The inverse of the function $F(x;t)$ defined in equation (18) is plotted here, for $x > x_{max}$ vs x^4 in the case of the quench to P_4. The full ovals correspond to $t = 1519\,\alpha^{-1}$, the empty ovals to $t = 1926\,\alpha^{-1}$, the full circles to $t = 2344\,\alpha^{-1}$, and the empty circles to $t = 3146\,\alpha^{-1}$. The dashed straight line corresponds to the dotted line in Fig. 7. It is seen here that $F(x;t) \simeq F(x) \sim x^{-4}$ describes approximately our data at values of $x \gtrsim x_{max}$ while at larger values of x, where scaling does not yet hold in our simulations, $F(x;t)$ is time dependent.

about the analytic form of the behavior of $k_1(t)$ for late times. This we have in common with real experiments—almost any assumed form with some adjustable parameters, can be made to fit the data. The results of our analysis are summarized in Table 3 and in Fig. 15. See also discussion in next section about the growth of clusters.

3.3 *Qualitative properties of the cluster distribution*

We define a *cluster* in our model system as a group of A atoms linked together by nearest-neighbor bonds. This is expected to correspond, approximately, at low concentrations of the minority component, to the grains observed by microscopy in real materials; it is the latter which the conventional nucleation theories have in mind and about which we would like to obtain information from our simulations [2, 7f, 16]. The computer was programmed to record periodically the 'sizes' and 'energies' (i.e. the surface areas defined as the total number of A–B bonds incident on the cluster) of all the clusters in the current configuration. The size of a cluster, l, is defined as the number of A atoms in the cluster.

A qualitative description of the (early) time evolution of the cluster distribution $n(l, t)$, the total number

Table 3.

Phase point		Maximum duration of run	$k_1 \sim t^{-a}$ a	$k_1^{-3} = A + Bt/10^3, t \geq t_0$ A	B	t_0
P_1	0.59 T_c 5%	14,000	0.35	8.8	1.5	6800
P_2	0.59 T_c 7.5%	10,200	0.23	7.5	1.5	4000
P_3	0.59 T_c 10%	7300	0.21	3.6	1.5	2500
P_4	0.59 T_c 20%	3900	0.19	2.3	1.7	1500
P_5	0.59 T_c 50%	650	0.19	1.2	3.0	350
P_6	0.78 T_c 50%	1700	0.23	1.4	3.0	1000
P_7	0.89 T_c 50%	6600	0.25	3.5	3.9	1000

Values of the adjustable parameters for two different fits to k_1: first assuming a simple power law (here all the data except the very early one is included in the fit), and then assuming a linear behavior of k_1^{-3} with time (using only data for $t \geq t_0$). Here t_0 is the approximate time at which we observed the onset of the dynamical scaling of the structure function according to equation (15).

of clusters of size l, has been reported elsewhere [7e] for the case $T \simeq 0.6\ T_c$. For values of ρ very close to ρ_v, the corresponding saturated vapor density, $n(l, t)$ rapidly settles down to a stationary value characteristic of a metastable state. At $\rho \simeq 0.05 - 0.075$ the distribution of 'small' clusters still approaches rapidly a quasi-stationary distribution characteristic of metastable states, but there is now a measurable rate at which larger clusters develop (i.e., a finite nucleation rate). A detailed quantitative analysis of this behavior, at $\rho = 0.075$, using ideas from the Becker–Döring and Lifshitz–Slyozov nucleation theory is given in Refs. [7f] and [16]. As the density (and the supersaturation) is increased further, $\rho \gtrsim 0.1$ at $0.6\ T_c$, we observe the early appearance of relatively large loose clusters ($l > 50$) coexisting with very small clusters of size one to ten or so. The number of A atoms and their relative distribution in the small clusters is close to what is observed in the A-poor (*gas*) phase equilibrium state. The system then shows a slow process of aggregation of the larger clusters into still larger compact clusters which will finally lead to a fully segregated A-rich (*liquid*) phase [5, 16]. When the density of A atoms in the model system is increased further, the system undergoes *percolation*, i.e. the appearance of 'infinite' size clusters. This happens in our model system (simple cubic lattice) at approximately [17] $\rho = 0.31$ for atoms placed entirely randomly on the lattice (i.e., $T = \infty$), and was also observed [7a, 7c] at $P_4 - P_7$. To our knowledge this phenomena has not been investigated so far in real alloys.

A detailed analysis of the cluster distribution $n(l, t)$ at low densities will be reported elsewhere [16] on the basis of a kinetic theoretical model of the Becker–Döring type. We shall only report here some gross features of $n(l, t)$ as one varies ρ at $T \simeq 0.6\ T_c$, namely on the time evolution of the cluster mean size defined as

$$l_i(t) = \sum_{l>l_c} l^i n(l,t) \Big/ \sum_{l>l_c} l^{i-1} n(l,t), \quad i = 1, 2. \qquad (20)$$

The cut-off l_c is intended as a (somewhat arbitrary) separation between 'small' and large clusters. The second of these definitions (note that the notation differs from that for k_1 and k_2 in equation (14)) gives more weight to large l and diminishes to some extent the relevance of the choice l_c. We present in Fig. 11 a plot of $l_2(t)$ vs time for $l_c = 20$ (similar results are obtained for $l_c = 50$) for quenches to P_1–P_3. There is clearly a difficulty in analysing these data on the assumption of a simple power law [5] behavior with time as suggested by the Lifshitz–Slyozov theory [2]. This may however be due to the fluctuations in our single run.

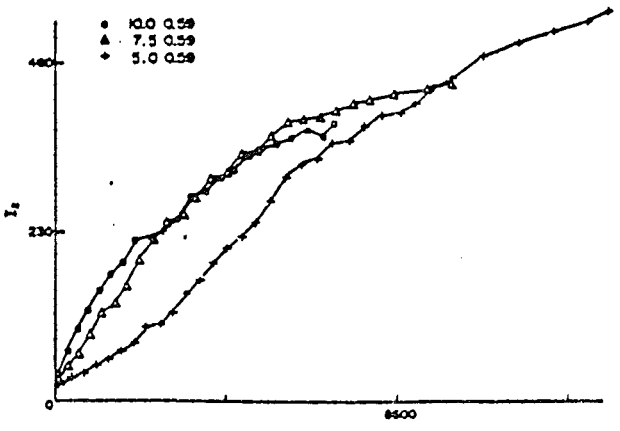

Fig. 11. The mean size $l_2(t)$, as defined in equation (20) with $l_c = 20$, is plotted here vs time (in units of α^{-1}) for the cases P_1 (crosses), P_2 (triangles) and P_3 (circles).

We find that the ratio $\langle l^2\rangle/\langle l\rangle^2 = l_2/l_1$, which gives information about the shape of the cluster distribution $n(l, t)$, is far from constant even for late times—unlike the corresponding quantity $\langle k^2\rangle/\langle k\rangle^2$ obtained from the structure function $S_1(k, t)$. Moreover even when the cluster distribution of the system changes dramatically as a consequence of the percolation phenomena mentioned earlier we do not observe a clear evidence of this change on the behavior of $S(k, t)$; e.g. the same scaling properties seem to hold for $\rho \leqslant 0.1$ and for $\rho \geqslant 0.2$. This is perhaps not so surprising since it is known that when the system undergoes percolation at high temperatures ($T \gg T_c$) there is no corresponding change in the equilibrium structure function [7, 17]. Thus it seems that attention must be paid not only to the size but also to the 'shapes', composition and distribution of the clusters and other properties of the system. Note, however, that it is possible to make other definition of 'clusters' to avoid the trouble with the percolation of clusters [5].

We finally mention that the theoretical ideas about scaling with time of $S(k, t)$ (section 2.2) are based on the assumption [5, 6] that for late times after quenching (to temperatures far enough from T_c) the mean 'diameter' R of the grains is much larger than the (thermal) correlation length. Thus R is the only relevant length scale for fluctuations in these circumstances and the structure function should be scaled accordingly. Moreover when ρ is small and the temperature is low one may assume nearly pure grains of the minority (A) phase so that $R^3(t)$ is approximately proportional to $l_1(t)$ and one is lead to the prediction $k_1(t) \sim [l_1(t)]^{-1/3}$. This is confirmed by Fig. 12 where we have plotted $k_1^{-3}(t)$ versus $l_1(t)$.

3.4 *Comparison with experiment*

3.4.1. *Preliminary remarks.* The model used in our computations certainly involves a great over-simplification of the behavior of real alloys where the processes we are interested in are greatly influenced by elastic distortions, grain boundaries, vacancies and other competing phenomena. The behavior of the model can thus only be compared with that of real materials in highly idealized conditions. Despite this, previous analysis have shown that our results are frequently very similar to experimental observations [7d]. In order to make comparison with experiments, however, care must be paid to the relation between the units and other characteristics in our model and those corresponding to real alloys. For instance, as described before, the basic unit of time α^{-1} for the model evolution may correspond in real alloys to times which vary between very broad limits: e.g. from $\alpha^{-1} \sim 50$ s at 0.6 T_c to 10^{-4} s at 0.8 T_c in the case of alluminum alloys. Thus our simulations at 0.6 T_c can be compared with experimental observations on real alloys (where the system relaxation is typically followed for some hours) while one has to be cautious at higher temperatures, say 0.8 T_c.

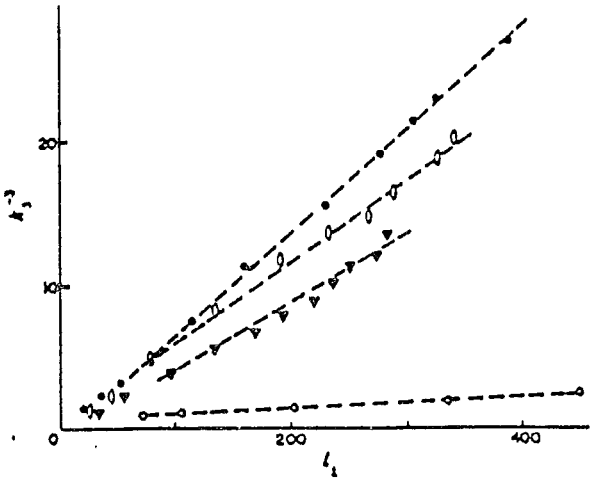

Fig. 12. Plot of $k_1^{-3}(t)$ [see equation (14)] vs $l_1(t)$ see equation (21) in the case of quenches to P_1 (full circles), P_2 (stars), and P_3 (triangles). A part of the case corresponding to P_4 (empty circles), where percolation effects were present, is also shown. The cut-off is $l_c = 20$ for the data at P_1–P_3 and $l_c = 10$ for P_4.

We note further that the typical resolution of X-ray cameras is in the range [21] of 10–1000 Å and that the inhomogeneities measured by experimentalists, e.g. the so-called 'Guinier–Preston zones', have typically linear dimensions in the range 15–200 Å. Thus, assuming $a_0 = 3$ Å the smallest grains measured in typical experiments contain between 30 and 150 atoms, and the largest ones about 3×10^5 atoms. This may influence the comparison between experiments and simulations given the cut-off l_c in equation (20) and given that the largest clusters observed in our simulations at P_1–P_3 contain typically no more than 800 A-atoms [23].

Other causes of differences between the behavior of our model and experimental observations can be found in the quenching rate which is finite in real experiments but infinite in our model system. We have checked that the quenching process seems to influence considerably the subsequent evolution. For instance we have been able to reproduce qualitatively the 'untypical' observations by Allen *et al.* [19], corresponding to room temperature aging of Al–Zn, $\rho = 0.12$, quenched into iced water ($T \simeq 0.44\ T_c$) from $T \simeq 0.93\ T_c$, by simulating a similar double quenching of our model system. The influence of the quenching process has also been reported in the case of some liquid mixtures [20].

3.4.2 *Comparisons.* We have analysed the data reported by Singhal, Herman and Kostorz [10] corresponding to the Au–60 at.% Pt alloy, in particular their Fig. 3 coming from an experiment in which the sample was solutionized at around 1543 K and then quenched into iced brine; the aging at around 823 K was observed by neutron scattering during 900 s. The composition of the sample lies at the center of the miscibility gap, and $T \simeq 0.6\ T_c$ so that the experiment may be compared with our simulations at P_5 and perhaps at P_4. Moreover, those authors estimate [10] the interdiffusion coefficient as being of order

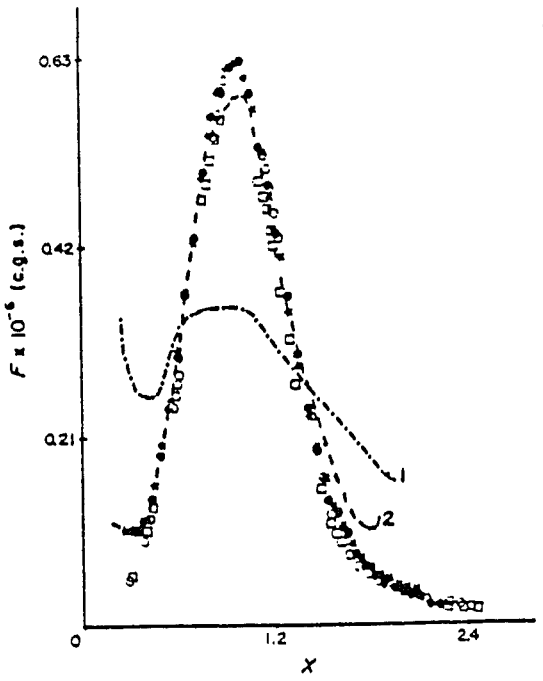

Fig. 13. We compare in this figure data from the computer simulation (empty symbols) with the experimental data in Fig. 3 from Ref. [10] (full symbols) corresponding to Au–60 at.% Pt alloy quenched to $T \simeq 0.6\ T_c$. The full circles are for $t = 900$ s and the stars for $t = 360$ s, both lying on the same curve except perhaps for $x \gtrsim 1.8$. The broken line 1 is for $t = 0$ (the initial sample was already decomposed to some extent), and the broken line 2 is for $t = 30$ s, in both cases scaling does not yet hold. The empty circles correspond to our simulation at P_3 while the empty squares are for P_4 (see Fig. 7). Only the vertical scale in Fig. 7 needed to be changed in order to obtain the present fit.

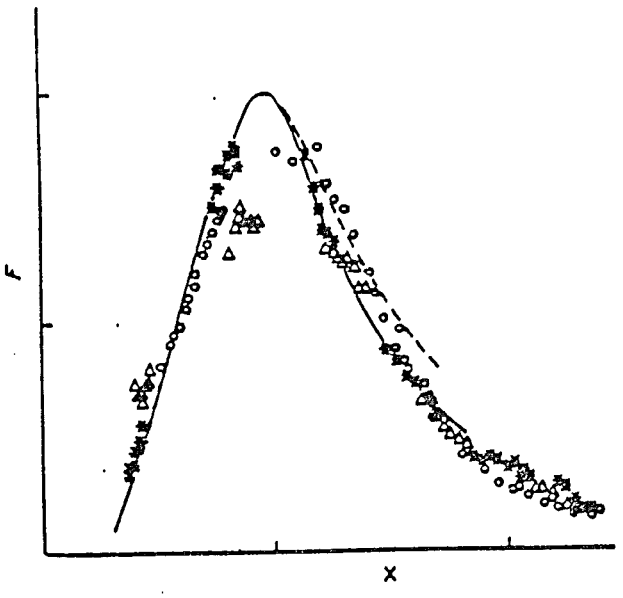

Fig. 14. The data in Fig. 9 is compared with experimental data (Ref. [11]) on an Al–15% Zn alloy quenched to 90°C (solid line) and to 110°C (dashed line) (both $T \simeq 0.6\ T_c$). The vertical and horizontal scales in Fig. 9 where changed to obtain the present fit; a fairly good fit can also be obtained, however, by changing only the vertical scale in Fig. 9.

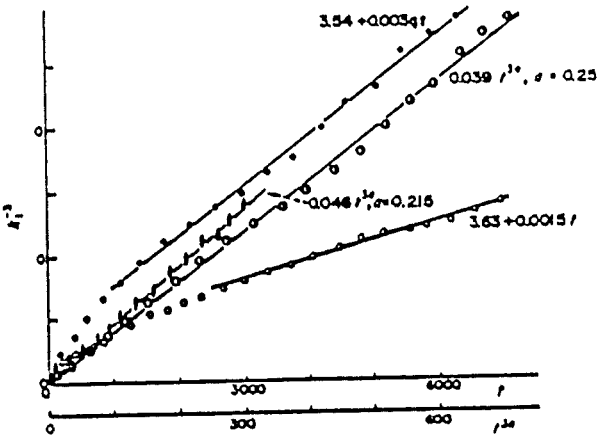

Fig. 15. This is a comparison of the fits reported in Table 3: k_1^{-3} is plotted here versus t and vs $t^{1/3}$ in the case of quenches to P_3 (empty circles and stars, respectively) and to P_7 (full circles and circles with a star, respectively). The straight lines correspond to fits of the form $k_1^{-3} = A + Bt$ and $k_1^{-3} = Ct^{1/3}$, as indicated.

10^{-16} cm^2/s at 823 K; choosing (arbitrarily) $a_0 = 3$ Å we have $\alpha^{-1} \sim 0.75$ s so that the duration of our evolution at P_3 is equivalent to about 500 s in terms of 'real' time (and to about 3000 s at P_4). The scattering analysis gives a structure function with a shape quite similar to the one observed in our simulations, including the characteristic crossovers at that temperature and composition in the tail, $k > k_{max}$.

We have also computed the function $F(x, t)$ defined in equation (18) taking as $S_1(k, t)$ the experimental data in Fig. 3 of Ref. [10]. We find that the data satisfy the scaling hypothesis in the time range $120\text{ s} \leqslant t \leqslant 900$ s for all but very large x, say $x > 1.8$, see Fig. 13. Indeed the experimental function $F(x)$ is quite similar to the corresponding one in the case of our simulations at P_4 and P_5. In fact one can make the data from the actual and computer experiments lie on the same curve by only re-scaling the vertical axis, as seen in Fig. 13. Additional data taken from this experiment is given at the end of Table 1. The area under $\mathcal{S}(k, t)$, for $0.03 \leqslant k \leqslant 0.21$ Å^{-1}, is seen to grow with time as is found in our simulations. On the other hand the shifting of the location and increase in length of the peak of $\mathcal{S}(k, t)$ is slower than in the case of our simulations. This might be due to the slow cooling process followed in Ref. [10] (as compared to our instantaneous quenching); in fact those authors report that the sample decomposed to some extent during the quenching process; and we may note that their $\mathcal{S}(k, t)$ at $t = 0$ is about twice as high for $k \simeq 0.1$ Å^{-1} than for $k \simeq 0.2$ Å^{-1} (instead of being approximately constant).

We have found a similar agreement between our scaling function $F(x)$ at P_1 and P_2, and the one reported by Guyot *et al.* [11] corresponding to a sample of Al–15 at.% Zn quenched to $T \simeq 0.6\ T_c$; this is shown in Fig. 14.

Finally, recent observations on binary fluid mixtures [12, 20, 22] report a behavior which is also

qualitatively similar to the one shown by our model system (note, however, when making comparisons that the diffusion coefficient is much larger for fluids, 10^{-4}–10^{-6} cm^2/s, than for alloys).

In particular Chou and Goldburg [12] find a scaling behavior of $\mathcal{S}(k, t)$ with a function $F(x)$ which looks quite similar to our function.

Acknowledgements—J.M. acknowledges financial support from the Comité Conjunto Hispano Norteamericano para la Cooperación Científica y Tecnológica. We would like to thank W. Goldburg, P. Guyot and C. Knobler for telling us of their experimental results before publication. We also thank K. Binder for comments on the manuscript and particularly to O. Penrose who pointed out to us that the late time data is consistent with Lifshitz–Slyozov theory. J.L. wishes to thank E. Brezin and C. de Dominicis for their kind hospitality at Saclay where part of this work was done.

REFERENCES

1. For reviews see J. W. Cahn, *Trans. metall. Soc. AIME* [illegible] (1968); J. E. Hilliard, in *Phase Transformations* (edited by H. I. Aaronson), p. 497. American Society for Metals, Metals Park, Ohio (1970).
2. I. M. Lifshitz and V. V. Slezov, *J. Phys. chem. Solids* 19, 35 (1961).
3. H. E. Cook, *Acta metall.* 18, 297 (1970).
4. J. S. Langer, M. Bar-on and H. D. Miller, *Phys. Rev.* A 11, 1417 (1975), and references therein.
5. K. Binder and D. Stauffer, *Phys. Rev. Lett.* 33, 1006 (1974); K. Binder, *Phys. Rev.* B 15, 4425 (1977); K. Binder, C. Billotet and P. Mirold, *Z. Phys.* B30, 313 (1978).
6. H. Furukawa, *Phys. Rev. Lett.* 43, 136 (1979).
7. (a) J. Marro, A. Bortz, M. Kalos and J. Lebowitz, *Phys. Rev. B* 12, 2000 (1975); (b) M. Rao, M. Kalos, J. Lebowitz and J. Marro, *Phys. Rev. B* 13, 4328 (1976); (c) A. Sur, J. Lebowitz, J. Marro and M. Kalos, *Phys. Rev.* B 15, 3014 (1977); (d) For a review see K. Binder, M. Kalos, J. Lebowitz and J. Marro, *Adv. Colloid Interface Sci.* 10, 173 (1979); (e) M. Kalos, J. Lebowitz, O. Penrose and A. Sur, *J. Stat. Phys.* 18, 39 (1978); (f) O. Penrose, J. Lebowitz, J. Marro, M. Kalos and A. Sur, *J. Stat. Phys.* 19, 243 (1978).
8. J. Marro, J. Lebowitz and M. Kalos, *Phys. Rev. Lett.* 43, 282 (1979).
9. H. Furukawa, '*Dynamics of Phase Separation in Dissipative Systems and Fluids Mixtures*', preprint to be published in *Phys. Rev. A*.
10. S. P. Singhal, H. Herman and G. Kostorz, *Neutron Small Angle Scattering Study of Phase Decomposition in Au-Pt*, preprint.
11. P. Guyot *et al.*, private communication; H. Hennion, D. Ronzand et P. Guyot, *Demixion des Solutions Solides Binaires: cas de Al–Zn*, preprint.
12. Y. C. Chou and W. I. Goldburg, *Angular Distribution of Light Scattered from Critically Quenched Liquid Mixtures*, 1980 preprint; C. M. Knobler, private communication.
13. K. Kawasaki, in *Phase Transitions and Critical Phenomena* (edited by C. Domb and M. S. Green), vol. 2. Academic Press, New York (1972).
14. J. W. Essam and M. Fisher, *J. chem. Phys.* 38, 802 (1963).
15. S. Fisk and B. Widom, *J. chem. Phys.* 50, 3219 (1969); D. Stauffer, *Z. Phys.* 221, 122 (1969); K. W. Sarkies and N. E. Frankel, *Phys. Rev.* A 11, 1724 (1975).
16. O. Penrose *et al.*, to be published. See also A. Buhagiar, Doc. Diss., Open University (1980).
17. A. Sur, J. Lebowitz, J. Marro, M. Kalos, and S. Kirkpatrick, *J. Stat. Phys.* 15, 345 (1976); see also J. Marro, Ph.D. Thesis, Yeshiva Univ. N.Y. (1975), University Microfilms, Ann-Arbor, Michigan (1976).
18. G. Laslaz, P. Guyot and G. Kostorz, *Decomposition Kinetics in Al-6.8 at.% Zn*, preprint; see also G. Laslaz and P. Guyot, *Acta met.* 25, 277 (1977).
19. D. Allen, J. Epperson, V. Gerold, G. Kostorz, S. Messoloras, and R. Stewart, *Neutron Small Angle Scattering Studies on Alluminium Alloys*, Conference on Neutron Scattering, Gatlingburgh, Tennessee, June (1976).
20. W. I. Goldburg, C. Shaw, J. S. Huang and M. S. Pilant, *J. chem. Phys.* 68, 484 (1978); see also W. I. Goldburg and J. S. Huang in *Fluctuations, Instabilities and Phases Transitions* (edited by T. Riste). Plenum Press, New York (1975).
21. For example V. Gerold, in *Small-Angle X-Ray Scattering* (edited by H. Brumberger). Gordon & Breach, N.Y. (1967), and references contained therein.
22. G. Morrison and C. M. Knobler, *J. chem. Phys.* 65, 5507 (1976); N. Wong and C. M. Knobler, *J. chem. Phys.* 66, 4707 (1977), and *Light Scattering Studies of Phase Separation in Isobutyric Acid + Water Mixtures*, preprint.
23. J. Vrijen, J. Aalders, C. van Dijk and S. Radelarr, *Phys. Rev. B* 22, 1503 (1980).